The Astrophysical Journal Letters, 724:L127–L132, 2010 December 1 doi:10.1088/2041-8205/724/2/L127

SOLAR WIND DRAG AND THE KINEMATICS OF INTERPLANETARY CORONAL MASS EJECTIONS

Shane A. Maloney and Peter T. Gallagher
School of Physics, Trinity College Dublin, College Green, Dublin 2, Ireland; maloneys@tcd.ie
Received 2010 July 29; accepted 2010 September 25; published 2010 November 8

ABSTRACT

Coronal mass ejections (CMEs) are large-scale ejections of plasma and magnetic field from the solar corona, which propagate through interplanetary space at velocities of ∼100–2500 km s^{-1}. Although plane-of-sky coronagraph measurements have provided some insight into their kinematics near the Sun (<32 $R_\odot$), it is still unclear what forces govern their evolution during both their early acceleration and later propagation. Here, we use the dual perspectives of the *STEREO* spacecraft to derive the three-dimensional kinematics of CMEs over a range of heliocentric distances (∼2–250 $R_\odot$). We find evidence for solar wind (SW) drag forces acting in interplanetary space, with a fast CME decelerated and a slow CME accelerated toward typical SW velocities. We also find that the fast CME showed linear ($\delta = 1$) dependence on the velocity difference between the CME and the SW, while the slow CME showed a quadratic ($\delta = 2$) dependence. The differing forms of drag for the two CMEs indicate the forces responsible for their acceleration may be different.

Key words: solar–terrestrial relations – Sun: activity – Sun: coronal mass ejections (CMEs)

Online-only material: color figures

1. INTRODUCTION

Massive eruptions of plasma and magnetic field that travel from the Sun through the heliosphere are known as coronal mass ejections (CMEs). CMEs can have masses up to 10^{16} g (Vourlidas et al. 2002) and propagate at velocities of up to 2500 km s^{-1} (Gopalswamy 2004) close to the Sun, while at 1 AU velocities tend to be closer to that of the solar wind (SW; Gopalswamy 2007). Although CMEs have been the subject of study for nearly 40 years, a number of fundamental questions regarding their acceleration and propagation remain unanswered. One such question, what forces govern the propagation of CMEs in the heliosphere, has been especially difficult to tackle. This is mainly due to a lack of three-dimensional (3D) observations of CMEs in the inner heliosphere.

The kinematic evolution of CMEs can be broken into three phases: initiation, acceleration, and propagation (Zhang et al. 2001). During the propagation phase, the initial acceleration has ceased and the CME motion is dominated by the interaction between the SW and the CME. The "snow plough," aerodynamic drag, and flux-rope models all aim to explain the motion of CMEs in the SW (Tappin 2006; Borgazzi et al. 2009; Vršnak et al. 2010; Cargill 2004; Chen 1996). An equation describing the motion of a CME in the drag-dominated regime may be written as

$$M\frac{dv}{dt} = -1/2C_D\rho_{\rm sw}A_{\rm cme}(v - v_{\rm sw})|v - v_{\rm sw}|, \quad (1)$$

where C_D is the drag coefficient, $\rho_{\rm sw}$ is the SW density, $A_{\rm cme}$ is the CME area, $v_{\rm sw}$ is the SW velocity, and M is the CME mass. We use a parametric drag model similar to that of Vršnak & Gopalswamy (2002) with the added parameter δ, which determines if the drag is quadratic or linear. This parametric form collapses the complex dependences of the CME area ($A_{\rm cme}$) and the SW density ($\rho_{\rm sw}$) into a power law which depends on heliospheric distance R. Equation (1) can thus be written as

$$\frac{dv}{dt} = -\alpha R^{-\beta}(v - v_{\rm sw})^{\delta}, \quad (2)$$

where α, β, and δ are constants.

Before the launch of the *STEREO* (Kaiser et al. 2008) mission, synoptic white-light CME observations were limited to 32 $R_\odot$ using LASCO (Brueckner et al. 1995), while the Solar Mass Ejection Imager (SMEI; Jackson et al. 2004; Howard et al. 2006) sometimes tracked CMEs to Earth (∼215 $R_\odot$). In radio observations, fast CMEs that drove shocks could be tracked to Earth (Reiner et al. 2007). Interplanetary Scintillation observation provided density and velocity measurements for both CMEs and the SW from 50 $R_\odot$ to beyond 1 AU, and using tomographic techniques can give 3D information (Manoharan 2006, 2010). CMEs are also observed with in situ *WIND* and *ACE* measurements at L1 (∼1 AU), and occasionally CMEs can be tracked up to very large distances of up to 5 AU using additional spacecraft (Tappin 2006). Numerical modeling has been used to study CME propagation with numerous approaches such as 1D Hydro simulations, 2.5D MHD simulations, and full 3D MHD simulations (González-Esparza et al. 2003; Cargill et al. 1996; Cargill & Schmidt 2002; Odstrčil & Pizzo 1999; Odstrčil et al. 2004; Smith et al. 2009; Falkenberg et al. 2010).

Statistical studies comparing in situ with white-light observations indicate a trend of CME velocity converging toward the SW velocity as they propagate to 1 AU (Gopalswamy 2007). Other studies, based on white-light observations have indicated that aerodynamic drag of some form may explain this trend (Vršnak 2001; Shanmugaraju et al. 2009). Radio observations suggest that a linear form of aerodynamic drag is most appropriate for fast CMEs (Reiner et al. 2003). Tappin (2006) showed that acceleration can continue far out (5 AU) into the heliosphere. However, these studies are subject to the difficulties associated with the observations they are based on. For example, white-light observations were limited to single, narrow, fixed, view points meaning only observation of the inner heliosphere could be made and even these were subject to projection effects (Howard et al. 2008a). Also, linking features in imaging and in situ observations is complex and can be ambiguous, a problem exacerbated during periods of high activity. In the case of numerical simulations, their complexity can make it hard to extract which effects are the most important, possibly obscuring the important underlying physics.

The unique *STEREO* mission consists of two nearly identical spacecraft in heliocentric orbits, *STEREO-B* (*Behind*) and *STEREO-A* (*Ahead*) which separate from the Sun–Earth line at 22.°5 per year. Each spacecraft carries the SECCHI (Howard et al. 2008b) suite, which images the inner heliosphere from the Sun's surface to beyond 1 AU. Using *STEREO* observations, a number of papers have been published which extract 3D information and study CMEs at extended heliocentric distances, overcoming some of the difficulties outlined above. Following Sheeley et al. (2008), Davis et al. (2009) used a constant velocity assumption and speed of a CME across Heliospheric Imager (HI1 and HI2) fields of view. The predicated arrival time, based on the speed derived, agreed with the in situ observations. Wood et al. (2009) used the "Point-P" and "Fixed-ϕ" methods to derive the height, speed, and direction from elongation measurements out to distances of $\sim$120 $R_\odot$. A recent paper by Liu et al. (2010) tracked a CME to $\sim$150 $R_\odot$ in 3D using J-maps from both spacecraft to triangulate the CMEs position in 3D. On the other hand, Maloney et al. (2009) tracked the trajectory of CME apexes in 3D using triangulation, some as far as 240 $R_\odot$. Byrne et al. (2010) developed a new reconstruction method which allowed the entire CME front to be reconstructed. They found evidence for CME deflection, expansion, and acceleration low down ($<$7 $R_\odot$) followed by a SW drag interaction. For a review of some of the different 3D reconstruction methods which have been applied to *STEREO* CME observations see Mierla et al. (2010).

In this Letter, we use triangulation to localize CME apexes in 3D. From this, we derive the CME apex trajectory and kinematics. These kinematics are then used to investigate the effects of drag on the CME. We present the reconstructed CME (apex) kinematics for three events: one accelerating, one decelerating, and one with constant velocity. In Section 2, we describe the observations, data reduction, and the reconstruction and fitting technique. Section 3 includes a discussion of each event in detail and presents the reconstructed kinematics themselves. The implications of our results and our final conclusions are given in Section 4.

2. OBSERVATIONS AND DATA ANALYSIS

2.1. Observations

The trajectories of three CMEs were reconstructed using observations from *STEREO* SECCHI. SECCHI consists of five telescopes: the Extreme Ultraviolet Imager (EUVI), the inner and outer coronagraphs (COR1 and COR2, respectively), and finally HI1 and HI2. COR1 images the corona from 1.4 to 4.0 $R_\odot$, while COR2 images the corona from 2.5 to 15 $R_\odot$. Both of the coronagraphs take sequences of three polarized images which can be combined to give total brightness (B) or polarized brightness (pB) images (Howard et al. 2008b; Thompson et al. 2003). The HI instrument is a combination of two refractive optical telescopes with multi-vein, multi-stage light rejection system which images the inner heliosphere from 4° to 89° (Eyles et al. 2008). HI1 images the inner heliosphere from 3.°98 to 23.°98 (degrees elongation) in white light with a cadence of 40 minutes, while HI2 images the heliosphere from 18.°68 to 88.°68 in white light with a cadence of two hours.

The three CMEs considered here were observed during 2007 October 8–13 (CME 1), 2008 March 25–27 (CME 2), and 2008 April 9–12 (CME 3). The observations were reduced using *secchi_prep* from the SolarSoft library (Freeland & Handy 1998). This consisted of debasing and flat fielding for all images. The COR1 and COR2 images were also corrected for vignetting, exposure time, and an optical distortion. The COR1 observations had a model background subtracted to remove static coronal features. The HI instrument has no shutter, and as such, these observations needed additional corrections for smearing and pixel bleeding. The pointing of the HI observations was updated using known star positions within the filed of view (Brown et al. 2008). Standard running difference images were created from the COR1/2 observations while a specialized running difference technique was used to suppress the stars for the HI observations (Maloney et al. 2009). The relative drift, due to satellite motion, of the star field between two successive HI images is calculated and then the earlier image is shifted to account for this motion removing a large part of the background signal. Figure 1 shows reduced observations from the 2008 March 28 event where the CME is simultaneously observed in both COR1 and COR2 in both the *STEREO-A* and *STEREO-B* spacecraft but only in from the *STEREO-A* spacecraft in HI.

2.2. 3D Reconstruction

Each event was observed in either COR1 or COR2 simultaneously by both *STEREO-A* and *STEREO-B*. From these images, the CME apex was localized via tie pointing (see Maloney et al. 2009, Figure 1; Inhester 2006). The trajectory was then reconstructed by tracking it through a series of images. In all of the events presented, the CME was only observed in HI by one spacecraft, so an additional constraint was required to localize the CME apex. We therefore assumed that the CME continued along the same path with respect to solar longitude, as it did in the COR1/2 field of view (i.e., traveled radially; Maloney et al. 2009). Figure 2 shows the derived trajectory for the 2008 March 25 event. Once the 3D trajectories were derived, we calculated the height and then took numerical derivatives with respect to time to obtain the velocity and acceleration.

2.3. Kinematic Modeling

The kinematics were fitted, via a least-squares method, with a parametric model for the drag (Equation (2)). In order to test which form of drag was most suitable (linear or quadratic), we fitted (Equation (2)) with δ set to 1 and then separately with δ equal to 2. The kinematics were only fit during the time interval, we believe that drag is at play and the observations are accurate. There was evidence for an early acceleration phase not attributed to drag which was not fitted. Also, events which were tracked far into HI2 field of view where identification of the CME apex becomes ambiguous were excluded from fitting.

A number of the model parameters can be fixed from the observations, such as the CME height and velocity. We assume that the CME velocity tends toward the SW speed, which was taken to be where the velocity plateaus. The model parameters obtained from the fitting were then compared with previous results from Vršnak & Gopalswamy (2002). From this comparison, we infer which model best reproduces the kinematics and hence is the most appropriate. Both the fast and slow CMEs (CME 1 and CME 2) were analyzed using this method. The intermediate CME (CME 3) was fitted with a constant acceleration model to show that there was no significant acceleration involved.

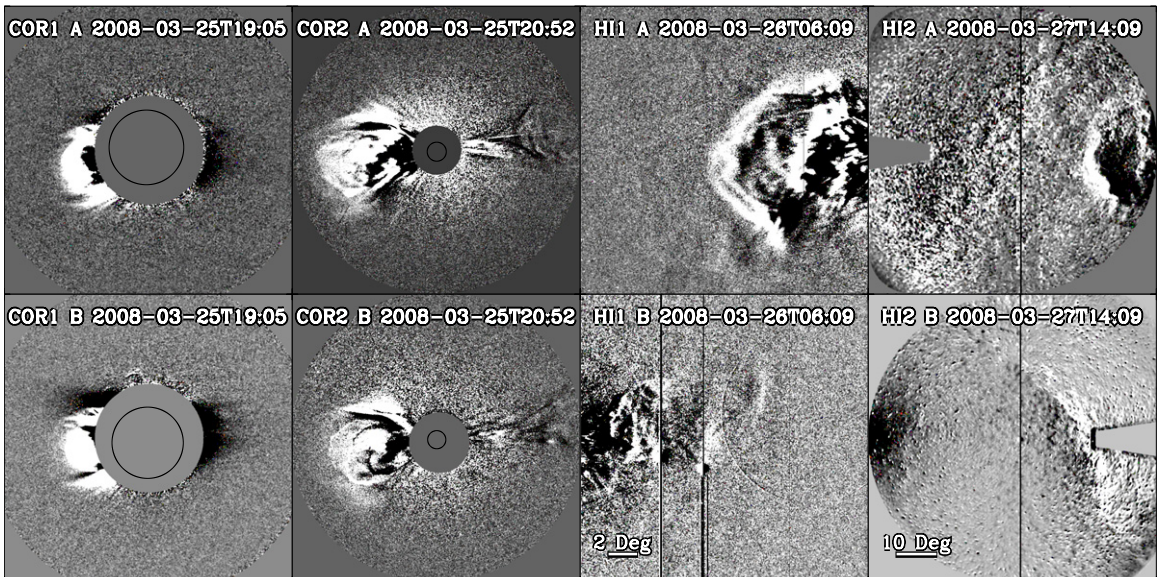

Figure 1. Sample images of the 2008 March 25 event showing the CME in COR1, COR2, HI1, and HI2 fields of view. Observed from *STEREO-A* (top row) and from *STEREO-B* (bottom row). Note the absence of a clear CME signature in the *STEREO-B* HI1 and HI2 images.

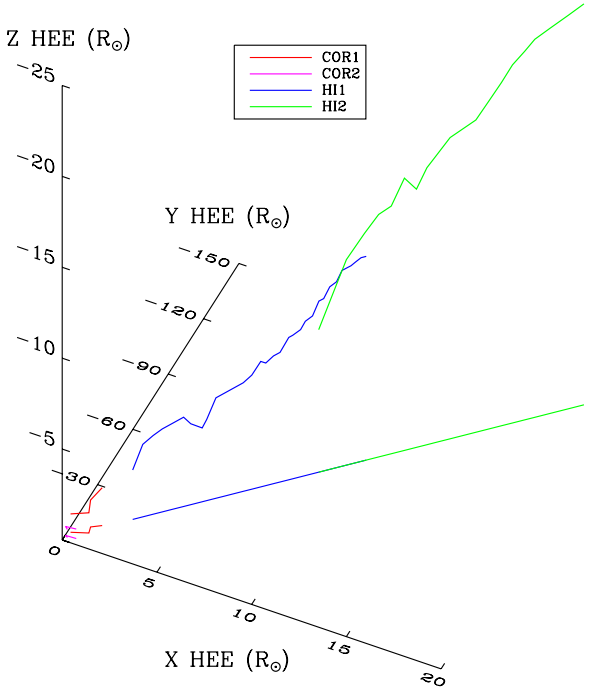

Figure 2. Reconstructed apex trajectory of the 2008 March 25 CME. The CME is tracked through COR1, COR2, HI1, and HI2 fields of view. For the COR1 and COR2 observations the CMEs' position is reconstructed using triangulation. In the H I field of view, we assume that the CME will continue along the same path as it did in COR1 and COR2 (traces in the *x*–*y* plane) in order to determine the CMEs' position in 3D space. The *x*-axis points toward the Earth, the *y*-axis is perpendicular to the *x*-axis and in the ecliptic plane, the *z*-axis is perpendicular to both.

(A color version of this figure is available in the online journal.)

3. RESULTS

CME 1 and CME 2 were fit in three ways with α, β, and δ all allowed to vary (black line), with fixed δ of two (magenta line) and one (orange line). In both cases, the free fitting returned values that were not comparable to previous studies (Vršnak 2001). The different fit parameters for the events are given in Table 1. CME 3 was fit with a constant acceleration model (black line).

Table 1
Fit Parameters for the Accelerating Events

Event and Model	α	β	δ	χ^2
CME 1 (2007 oct 8)				
Linear (magenta)	1.61e-5	−0.5	1.0	8.27
Quadratic (orange)	1.28e-7	−0.5	2.0	6.74
CME 2 (2008 Mar 25)				
Linear (magenta)	1.02e-4	−0.5	1.0	3.71
Quadratic (orange)	6.38e-7	−0.5	2.0	17.63

Notes. CME 1, $v_{sw} = 450$ km s^{-1}, $v_{cme} = 233$ km s^{-1}, $h_0 = 12\ R_\odot$. CME 2, $v_{sw} = 325$ km s^{-1}, $v_{cme} = 702$ km s^{-1}, $h_0 = 44\ R_\odot$.

3.1. CME 1 (2007 October 8–13)

Figures 3(a)–(c) show the kinematics for the accelerating CME. This CME was first observed at 15:05 UT on 2007 October 8 off the west limb and was found to be propagating at an angle of 56° from the Sun–Earth line. Figure 3(a) shows the height of the CME. Figure 3(b) shows the velocity profile which clearly shows that the CME is undergoing acceleration, initial velocity of ∼150 km s^{-1} and final velocity of ∼450 km s^{-1}. There may be two acceleration regimes, an early increased acceleration phase (before 18:00 UT on the October 8) followed by a drag acceleration. The early acceleration can be attributed to a magnetic driving force and so was not fitted with the drag model. Later, when the CME reached the center of the HI2 field of view, determining the front position becomes difficult so this region was not fitted. Figure 3(c) shows the acceleration profile of the event. The $\delta = 2$ (orange) fit gives the lowest chi-squared value.

3.2. CME 2 (2008 March 25–27)

The kinematics from the decelerating CME are shown in Figures 3(d)–(f). This CME was first observed at 18:55 UT on 2008 March 25 off the east limb and was found to be propagating at an angle of −82° from the Sun–Earth line. Figures 3(d)

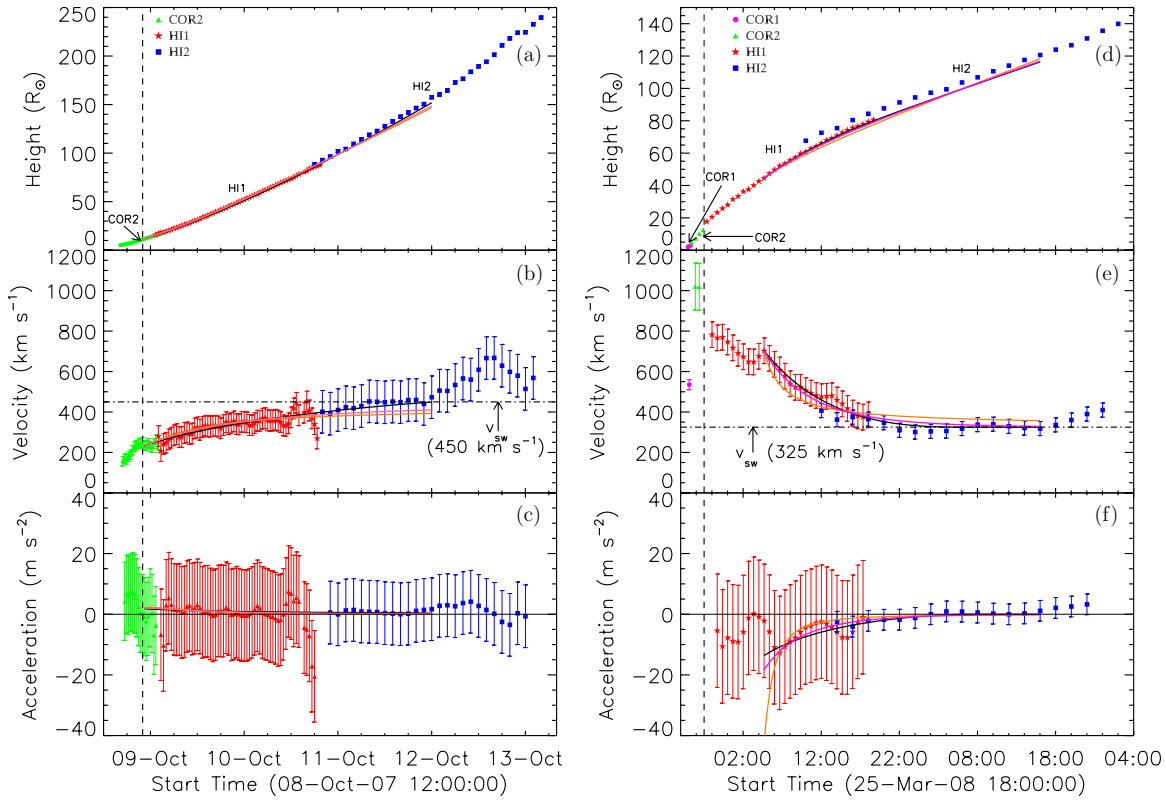

Figure 3. Left panel: kinematics for CME 1, (a) height, (b) velocity, and (c) acceleration. Right panel: kinematics for CME 2, (d) height, (e) velocity, and (f) acceleration. Vertical dashed line indicates separation between early- and late-phase acceleration. Horizontal dot-dashed line indicates the inferred SW velocity.
(A color version of this figure is available in the online journal.)

and (e) show the height and velocity profiles, the velocity profile clearly demonstrates that the CME is undergoing deceleration. The CME had an initial velocity (HI1) of ∼800 km s^{-1} and a final velocity of ∼375 km s^{-1}. Due to the high speed of this CME, it was only observed in a small number of frames in COR1 and COR2. As a result, the kinematics were difficult to quantify in these instruments. However, there appears to have been an early acceleration feature. The deceleration in the HI1 and HI2 fields of view continued until the CME reached a near-constant velocity and traveled at this velocity throughout the rest of the field of view. Figure 3(d) shows the acceleration profile of the event. The $\delta = 1$ (magenta) fit gives the lowest chi-squared value.

3.3. CME 3 (2008 April 9–12)

In Figure 4, we show the kinematics of the constant velocity CME. This CME was first observed at 15:05 UT on 2008 April 09 off the east limb and was found to be propagating at an angle of −73° from the Sun–Earth line. Figure 4(a) shows the height of the CME. Figure 4(b) shows the velocity profile which has a scatter about ∼300 km s^{-1}. Again, there may be some evidence in the COR1/2 observations for an early acceleration phase but due to the event's poorly observable features, at this early stage, it is hard to quantify this. The departure from the fit after April 12 20:00 UT is thought to be due to error in the reconstruction as the CME apex becomes too faint to identify. As this event shows no obvious acceleration, it was not fitted with the drag model but with a constant acceleration model $h(t) = h_0 + v_0 t + 1/2at^2$ (thin black line). Figure 4(c) shows the acceleration profile, the fit values ($h_0 = 22\ R_{\rm Sun}$, $v_0 = 334$ km s^{-1}, and a $= -0.18$ m s^{-2}) are consistent with no acceleration throughout the field of view.

4. DISCUSSION AND CONCLUSIONS

We have shown that it is possible to derive the 3D kinematics of features, the CME apex in this case, in the inner heliosphere (∼2–250 $R_\odot$) using *STEREO* observations. The 3D kinematics are free from the projection effects of traditional 2D kinematics but may contain artifact from the 3D reconstruction method (e.g., Maloney et al. 2009) and other sources. Both of the accelerating events showed two regimes in the velocity profile, a low down (<15 $R_\odot$) early rapid acceleration (in comparison to later values), followed by a gradual acceleration far from the Sun (>30 $R_\odot$). The early acceleration is thought to be due to a magnetic driving force, as the SW velocity in the low corona is less than the CME velocity at <∼10 $R_\odot$, it is likely that the early CME acceleration results from magnetic rather than drag forces. Here, we assume that the later acceleration is due the interaction between the SW and the CME, as in each case the CME attains a final velocity close to typical values for the SW.

Considering CME 2 in Figures 3(d)–(f), it can clearly be seen that the velocity levels off to a constant value typical of the SW. We interpret this as the CME reaching the local SW speed, as a result the force acting on the CME goes to zero. For CME 1 (Figures 3(a)–(c)), the velocity initially increases, however, there is a plateau toward the end after April 11 6:00 UT which occurs at SW like speeds. The height measurements toward the end are very scattered and show rapid increase. This is most likely due to losing the front to the background noise and triangulating a different feature. CME 3 propagates at a roughly constant velocity, which is consistent with the drag interpretation. The CME appears to have already attained the local SW speed and therefore is not accelerated. The fitting results show that a linear dependence produces a better fit for

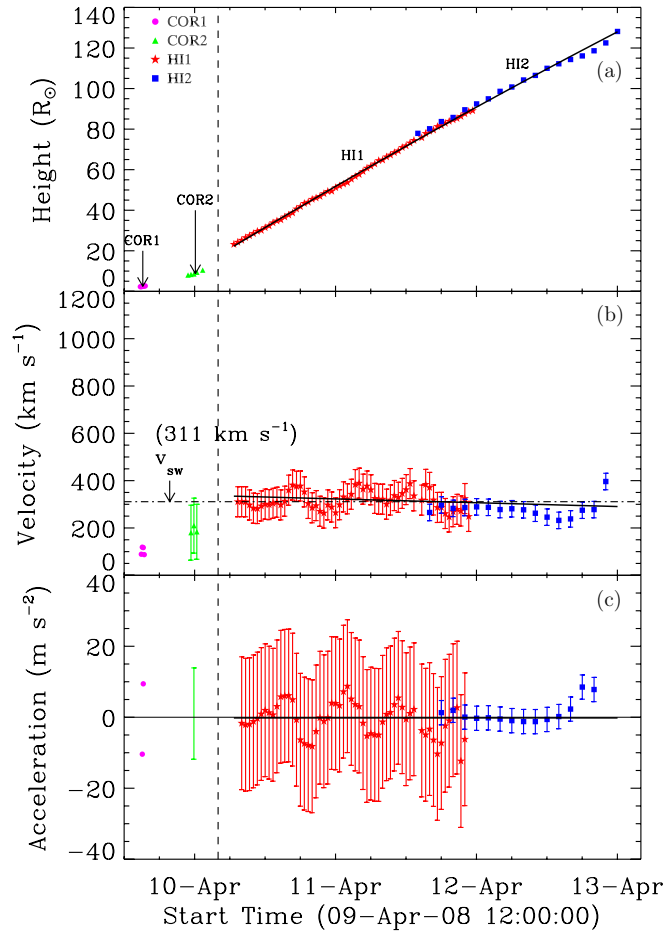

Figure 4. Kinematics for CME 3: (a) height, (b) velocity, and (c) acceleration. This event shows an early acceleration (to left if dashed line) which levels of to a scatter about typical SW speeds. This event was fit with a constant acceleration, the resulting fit parameters are $h_0 = 22\ R_{\rm Sun}$, $v_0 = 334$ km s^{-1}, and $a = -0.18$ m s^{-2}. The assumed SW value is indicated by the horizontal dot-dashed line.

(A color version of this figure is available in the online journal.)

the fast event (CME 2), while a quadratic dependence better fits the slow event (CME 1). The differing range of the interaction CME 1 $\sim$120 $R_\odot$ and CME 2 $\sim$ 80 $R_\odot$ may be explained by the suggestion that wide low-mass CMEs are more affected by drag than narrow massive CMEs (Vršnak et al. 2010).

Reiner et al. (2003) suggest that for fast events a linear model of drag better reproduces the kinematics, which agrees with our findings. Vršnak (2001) also suggested that a linear dependence might be appropriate, however the quadratic form has been studied much more. From a theoretical perspective, a quadratic dependence corresponds to aerodynamic drag, while a linear dependence suggests Stokes' or creeping drag. It is not currently clear which model is more physically correct. The fit parameters obtained do not agree with those found by Vršnak (2001) and while our values are not unphysical, it is not clear why they differ so much from the previous studies.

The mechanism behind the apparent differing forms of drag, linear ($\delta = 1$) and quadratic ($\delta = 2$), for the slow and fast events is unclear. The application of any hydrodynamic theory to a CME, such as drag, may be missing vital physics. Could the magnetic properties play a role modifying the form of the drag (reconnection, suppression of turbulence, wave energy transport)? For example, Cargill et al. (1996) showed that depending on the orientation of the flux rope and background magnetic field (aligned or non-aligned), the drag coefficient can vary between 0 and 3. They also found that the magnetic field of the flux rope is important in order for its survival as it propagates. Furthermore, it is not yet clear if the drag responsible for modifying the motion of CMEs in the SW is due to viscous-dominated Stokes' drag or turbulence-dominated aerodynamic drug. These questions can only be addressed with additional observations and modeling.

We have shown that it is possible to derive the true 3D kinematics for a number of CMEs in the inner heliosphere. Based on this, we have been able to conclusively show that CMEs undergo acceleration in the inner heliosphere, more specifically, that due to its range and strength this acceleration is believed to be the result of some form of drag. This drag acceleration has important implications for space weather predictions and for the analysis techniques which assume that CMEs travel at constant velocity through the heliosphere. The HI observations of CMEs in the heliosphere provide a unique and limited opportunity to study the propagation of CMEs and to understand the coupling between the SW and CMEs.

This work is supported by Science Foundation Ireland Grant No. 07-RFP-PHYF399. We also thank the *STEREO*/SECCHI consortium for providing open access to their data and technical support.

REFERENCES

Borgazzi, A., Lara, A., Echer, E., & Alves, M. V. 2009, A&A, 498, 885
Brown, D. S., Bewsher, D., & Eyles, C. J. 2008, Sol. Phys., 254, 185
Brueckner, G. E., et al. 1995, Sol. Phys., 162, 357
Byrne, J. P., Maloney, S. A., McAteer, R. T. J., Refojo, J. M., & Gallagher, P. T. 2010, Nat. Commun., 1, 74
Cargill, P. J. 2004, Sol. Phys., 221, 135
Cargill, P. J., Chen, J., Spicer, D. S., & Zalesak, S. T. 1996, J. Geophys. Res., 101, 4855
Cargill, P. J., & Schmidt, J. M. 2002, Ann. Geophys., 20, 879
Chen, J. 1996, J. Geophys. Res., 101, 27499
Davis, C. J., Davies, J. A., Lockwood, M., Rouillard, A. P., Eyles, C. J., & Harrison, R. A. 2009, Geophys. Res. Lett., 36, 08102
Eyles, C. J., et al. 2008, Sol. Phys., 254, 387
Falkenberg, T. V., Vršnak, B., Taktakishvili, A., Odstrčil, D., MacNeice, P., & Hesse, M. 2010, Space Weather, 8, 06004
Freeland, S. L., & Handy, B. N. 1998, Sol. Phys., 182, 497
González-Esparza, J. A., Lara, A., Pérez-Tijerina, E., Santillán, A., & Gopalswamy, N. 2003, J. Geophys. Res. (Space Phys.), 108, 1039
Gopalswamy, N. 2004, in The Sun and the Heliosphere as an Integrated System, ed. G. Poletto & S. T. Suess (INAF-Osservatorio di Arcetri; Dordrecht: Kluwer), 201
Gopalswamy, N. 2007, Space Sci. Rev., 124, 145
Howard, T. A., Nandy, D., & Koepke, A. C. 2008a, J. Geophys. Res., 113, 1104
Howard, T. A., Webb, D. F., Tappin, S. J., Mizuno, D. R., & Johnston, J. C. 2006, J. Geophys. Res., 111, 04105
Howard, R. A., et al. 2008b, Space Sci. Rev., 136, 67
Inhester, B. 2006, arXiv:astro-ph/0612649v1
Jackson, B. V., et al. 2004, Sol. Phys., 225, 177
Kaiser, M. L., Kucera, T. A., Davila, J. M., Cyr, O. C. S., Guhathakurta, M., & Christian, E. 2008, Space Sci. Rev., 136, 5
Liu, Y., Davies, J. A., Luhmann, J. G., Vourlidas, A., Bale, S. D., & Lin, R. P. 2010, ApJ, 710, L82
Maloney, S. A., Gallagher, P. T., & McAteer, R. T. J. 2009, Sol. Phys., 256, 149
Manoharan, P. K. 2006, Sol. Phys., 235, 345
Manoharan, P. K. 2010, Sol. Phys., 265, 137
Mierla, M., et al. 2010, Ann. Geophys., 28, 203
Odstrčil, D., & Pizzo, V. J. 1999, J. Geophys. Res., 104, 483
Odstrčil, D., Riley, P., & Zhao, X. P. 2004, J. Geophys. Res., 109, 02116

Reiner, M. J., Kaiser, M. L., & Bougeret, J.-L. 2003, in AIP Conf. Proc. 679, Solar Wind Ten: Proceedings of the Tenth International Solar Wind Conference, ed. M. Velli, R. Bruno, & F. Malara (Melville, NY: AIP), 152
Reiner, M. J., Kaiser, M. L., & Bougeret, J.-L. 2007, ApJ, 663, 1369
Shanmugaraju, A., Moon, Y.-J., Vrsnak, B., & Vrbanec, D. 2009, Sol. Phys., 257, 351
Sheeley, N. R., et al. 1997, ApJ, 484, 472
Sheeley, N. R., et al. 2008, ApJ, 675, 853
Smith, Z. K., Steenburgh, R., Fry, C. D., & Dryer, M. 2009, Space Weather, 7, 12005
Tappin, S. J. 2006, Sol. Phys., 233, 233
Thompson, W., et al. 2003, Proc. SPIE, 4853, 1
Vourlidas, A., Buzasi, D., Howard, R. A., & Esfandiari, E. 2002, in Solar Variability: From Core to Outer Frontiers, The 10th European Solar Physics Meeting, ed. A. Wilson (ESA SP-506; Noordwijk: ESA), 91
Vršnak, B. 2001, Sol. Phys., 202, 173
Vršnak, B., & Gopalswamy, N. 2002, J. Geophys. Res. (Space Phys.), 107, 1019
Vršnak, B., Žic, T., Falkenberg, T. V., Möstl, C., Vennerstrom, S., & Vrbanec, D. 2010, A&A, 512, 43
Wood, B. E., Howard, R. A., Plunkett, S. P., & Socker, D. G. 2009, ApJ, 694, 707
Zhang, J., Dere, K. P., Howard, R. A., Kundu, M. R., & White, S. M. 2001, ApJ, 559, 452